Journal of Solid State Chemistry **145,** 479–483 (1999)
Article ID jssc.1999.8167, available online at http://www.idealibrary.com on IDEAL®

Weak Ferromagnetism and Framework Switching in $KMnHP_3O_{10}$

A. J. Wright,* C. Ruiz-Valero,† and J. P. Attfield*,[1]

*Department of Chemistry, University of Cambridge, Lensfield Road, Cambridge, CB2 1EW, United Kingdom; and
†Instituto de Ciencia de Materiales de Madrid, CSIC Campus de Cantoblanco, 28049 Madrid, Spain

Received September 17, 1998; in revised form December 27, 1998; accepted January 18, 1999

Polycrystalline $KMnHP_3O_{10}$ has been prepared from solution. It adopts a triclinically distorted variant of the $RbMnHP_3O_{10}$ structure and an approximate structure refinement has been obtained from powder neutron diffraction data (space group $P\bar{1}$, $a = 7.102(2)$, $b = 7.234(1)$, $c = 9.109(2)$ Å, $\alpha = 72.176(8)$, $\beta = 73.762(9)$, $\gamma = 70.642(12)^\circ$ at 2 K). A magnetic ordering transition is observed at 15 K, below which $KMnHP_3O_{10}$ displays weak ferromagnetism with a net moment of $\sim 0.3\ \mu_B$ per Mn ion showing that the true structural symmetry may be $P1$. The magnetic structure has an $a \times 2b \times 2c$ supercell and is more complex than that of the Rb and Cs analogues, due to a switching of the Jahn–Teller distortions of the MnO_6 octahedra. © 1999 Academic Press

INTRODUCTION

Transition-metal oxosalts exhibit a large variety of structures which give rise to magnetic exchange networks of different topologies and dimensionalities. Local electronic interactions such as Jahn–Teller distortions give further variety due to the "orbital ordering" of unpaired electrons in cooperatively distorted solids. Switching between different orbital orderings is known in coordination complexes, for example by the application of pressure to the Tutton Salt $(NH_4)_2Cu(H_2O)_6(SO_4)_2$ (1). Frameworks containing Jahn–Teller distorted polyhedra can also switch between distinct geometries by means of ion exchange, leading to the possibility of flexible host materials. This behavior was first demonstrated by Li^+/H^+ exchange in $MnAsO_4.H_2O$ (2), which produces a switch in the framework geometry, resulting from cooperative changes to the Jahn–Teller distortions of the MnO_6 octahedra. This change switches the Mn–O–Mn interactions from being antiferromagnetic in $MnAsO_4.H_2O$ to ferromagnetic in the derivative $LiMnAsO_4(OH)$ (3).

These switchable properties have led us to study the series of hydrogentriphosphates $AMnHP_3O_{10}$ (A = K, Rb, Cs) (4), which also contain high spin $3d^4$ Mn^{3+}. The structures and low temperature magnetism of the Rb (5) and Cs (6, 7) phases have recently been reported. Their structures are topologically equivalent although they have nonisomorphous C-centered monoclinic cells (Fig. 1). Strong symmetric P–O...H...O–P hydrogen-bonding links the HP_3O_{10} units into chains which are interlinked by the MnO_6 octahedra to form a three-dimensional framework with Rb or Cs cations occupying 10 coordinate sites within the channels. This can be contrasted to other $A^{I}M^{III}HP_3O_{10}$ materials, such as $NH_4AlHP_3O_{10}$ (8) and $CsGaHP_3O_{10}$ (9), which have the A cations separating layers of $HP_3O_{10}^{4-}$ anions and MO_6 octahedra.

Attempts to exchange H^+ with Li^+ always led to a collapse of the $AMnHP_3O_{10}$ frameworks, showing that the strong hydrogen bonding is essential to their stability, so that these materials do not act as chemically switchable frameworks. However, the dependence of the magnetic properties upon the large A cation can be investigated by comparing the three host structures. At low temperatures, both $RbMnHP_3O_{10}$ and $CsMnHP_3O_{10}$ show sharp antiferromagnetic transitions at 10 and 11 K, respectively (5, 7). Their magnetic structures (Fig. 1) are essentially identical despite the differences between their crystal structures. Ferromagnetically aligned planes of spins at $x = 1/4$ and 3/4 (using the $RbMnHP_3O_{10}$ cell axes) are coupled antiferromagnetically to each other. Here we report the preparation and magnetic behavior of the third phase, $KMnHP_3O_{10}$, and a preliminary study of its complex crystal and magnetic structures.

EXPERIMENTAL

$KMnHP_3O_{10}$ was prepared from an aqueous solution of K_2CO_3, Mn_2O_3, 85% H_3PO_4, and concentrated HNO_3 in a molar ratio of K:Mn:P:N = 9:2:30:10. This solution was heated to 250°C for 48 h and then slow cooled to room temperature over 12 h, after which the brown microcrystalline product was collected by filtration and washed with water. The product was characterized by powder X-ray

[1] E-mail: jpa14@cam.ac.uk.

0022-4596/99 $30.00

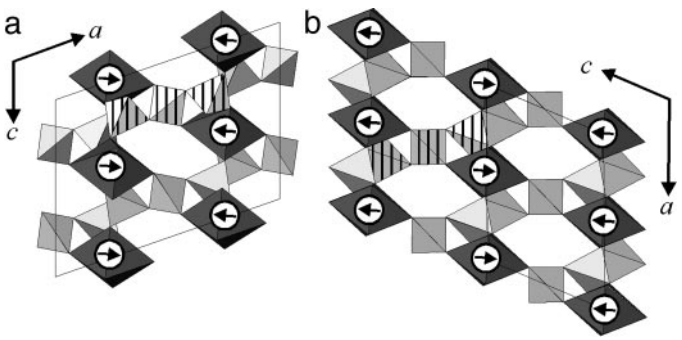

FIG. 1. [010] projection of the nuclear and magnetic structures of monoclinic (a) $RbMnHP_3O_{10}$ (C2/*c* symmetry) and (b) $CsMnHP_3O_{10}$ (C2 symmetry) showing their nuclear unit cells. Only the MnO_6 and PO_4 polyhedra are shown and a single P_3O_{10} unit is hatched in each case.

diffraction using Cu$K\alpha$ radiation. Attempts to prepare $NaMnHP_3O_{10}$ by the same method were unsuccessful.

Magnetic susceptibility data were recorded using a Quantum Design SQUID magnetometer. A 52.7 mg sample of $KMnHP_3O_{10}$ was initially cooled to 4 K in zero field and measurements were made while warming in fields of 0.05, 0.5, and 5 T.

Neutron powder diffraction data were collected at 2 and 150 K, with a wavelength of 2.4177 Å, for 40 min per pattern on the D20 instrument at ILL, Grenoble. This instrument contains a static bank of 1600 detectors in 0.1 intervals over the range 0–160 2θ. Rietveld analysis of the 2 K data was performed using the GSAS software package (10).

RESULTS

The powder X-ray diffraction pattern of $KMnHP_3O_{10}$ was indexed on a triclinic C-centered cell ($a = 11.765(2)$, $b = 8.331(1)$, $c = 9.155(1)$ Å, $\alpha = 91.57(1)$, $\beta = 111.14(1)$, $\gamma = 88.93(1)^\circ$) similar to that of monoclinic $RbMnHP_3O_{10}$ (5) showing that the structure is a triclinally distorted variant of the latter arrangement. A Rietveld fit to the 2 K neutron diffraction data was achieved with an asymmetry corrected pseudo-Voigt peak shape and a linear interpolated background function. The starting model for the nuclear fit was derived from the C2/*c* $RbMnHP_3O_{10}$ structure by transforming the coordinates to the primitive cell described by the vectors

$$\begin{pmatrix} \mathbf{a}_K \\ \mathbf{b}_K \\ \mathbf{c} \end{pmatrix} = \begin{pmatrix} 1/2 & -1/2 & 0 \\ 1/2 & 1/2 & 0 \\ 0 & 0 & 1 \end{pmatrix} \begin{pmatrix} \mathbf{a}_{Rb} \\ \mathbf{b}_{Rb} \\ \mathbf{c} \end{pmatrix}$$

(**c** is common to both structures and so is not subscripted), and lowering the symmetry to $P\bar{1}$. This produces several inequivalent sites which are labeled *a* and *b* in Table 1.

TABLE 1
Refined Structural Parameters for $KMnHP_3O_{10}$ obtained from Rietveld Analysis of 2 K Neutron Powder Diffraction Data in Space Group $P\bar{1}$ with e.s.d.'s in Parentheses

R factors (%): $R_{wp} = 3.6$ $R_p = 2.6$ R_{F^2} (nuc) = 6.0 R_{F^2} (mag) = 19.0
Lattice parameters: $a = 7.102(2)$ Å $b = 7.234(1)$ Å $c = 9.109(2)$ Å,
$\alpha = 72.176(8)^\circ$ $\beta = 73.762(9)^\circ$ $\gamma = 70.642(12)^\circ$

Atom	*x*	*y*	*z*
Mn(*a*)	0	0.5	0
Mn(*b*)	0.5	0	0.5
K	0.395(5)	− 0.444(5)	0.245(4)
P(1*a*)	0.249(4)	− 0.917(4)	0.243(3)
P(1*b*)	0.148(3)	− 0.727(3)	0.726(3)
P(2)	− 0.141(4)	− 0.869(4)	0.218(3)
O(1*a*)	0.031(3)	− 0.888(3)	0.279(3)
O(1*b*)	0.128(3)	− 0.939(4)	0.822(2)
O(2*a*)	0.251(4)	− 0.705(3)	0.136(2)
O(2*b*)	0.364(3)	− 0.754(3)	0.602(3)
O(3*a*)	0.381(4)	− 0.036(4)	0.139(3)
O(3*b*)	0.000(4)	− 0.618(3)	0.615(3)
O(4*a*)	0.275(4)	− 0.910(3)	0.419(2)
O(4*b*)	0.188(3)	− 0.589(3)	0.812(3)
O(5*a*)	− 0.139(4)	− 0.685(4)	0.058(2)
O(5*b*)	0.366(3)	− 0.173(3)	0.701(2)
H(1*a*)	0	0.5	0.5
H(1*b*)	0.5	0	0

Note. Overall $U_{iso} = 0.003(4)$ Å^2.

Attempts to fit the data by constraining the atomic positions using C/2*c* symmetry operations gave very poor agreement and in the final model all of the variable coordinates were refined independently in $P\bar{1}$. Results are displayed in Tables 1 and 2 and the fit is shown in Fig. 3.

TABLE 2
Bond Lengths (Å) for $KMnHP_3O_{10}$ obtained from Rietveld Analysis of 2 K Neutron Powder Diffraction Data, with e.s.d.'s in Parentheses

Mn(*a*)–O(2*a*)	(×2)	2.30(2)	P(1*a*)–O(1*a*)		1.45(3)
Mn(*a*)–O(4*b*)	(×2)	1.99(2)	P(1*a*)–O(2*a*)		1.55(3)
Mn(*a*)–O(5*a*)	(×2)	1.79(3)	P(1*a*)–O(3*a*)		1.41(3)
			P(1*a*)–O(4*a*)		1.68(3)
Mn(*b*)–O(2*b*)	(×2)	2.08(2)			
Mn(*b*)–O(4*a*)	(×2)	1.79(2)	P(1*b*)–O(1*b*)		1.54(3)
Mn(*b*)–O(5*b*)	(×2)	2.05(2)	P(1*b*)–O(2*b*)		1.62(3)
			P(1*b*)–O(3*b*)		1.52(3)
K-O(2*a*)		2.93(4)	P(1*b*)–O(4*b*)		1.58(3)
K-O(2*b*)		3.33(4)			
K-O(2*b*)		3.34(3)	P(2)–O(1*a*)		1.42(3)
K-O(3*a*)		2.78(4)	P(2)–O(1*b*)		1.51(3)
K-O(3*b*)		2.68(4)	P(2)–O(5*a*)		1.64(3)
K-O(4*a*)		3.53(4)	P(2)–O(5*b*)		1.54(3)
K-O(4*b*)		2.94(4)			
K-O(5*a*)		3.43(4)	H(1*a*)–O(3*b*)	(×2)	1.13(2)
K-O(5*a*)		3.45(3)			
K-O(5*b*)		2.71(3)	H(1*b*)–O(3*a*)	(×2)	1.32(2)

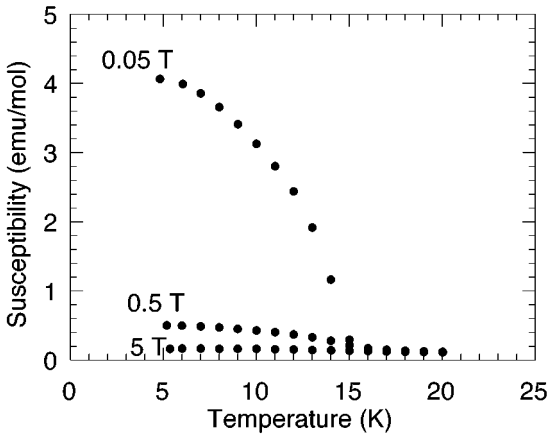

FIG. 2. Low-temperature magnetic susceptibility data for $KMnHP_3O_{10}$ measured in 0.05, 0.5, and 5 T fields.

The magnetic susceptibility data reveal a transition from paramagnetic to ordered behavior at $T_C = 15$ K. The field dependence of the susceptibility shows that there is a ferromagnetic component to the magnetic ordering (Fig. 2). The zero field saturated magnetic moment of $\sim 0.3\ \mu_B$ per Mn ion indicates that ferrimagnetic or weak ferromagnetic order occurs.

Long-range magnetic ordering is confirmed by the appearance of several magnetic diffraction peaks in the neutron diffraction pattern on cooling from 150 to 2 K (Fig. 3). These were indexed on an $a_K \times 2b_K \times 2c$ supercell and the magnetic intensities were fitted using the collinear model shown in Table 3 and a calculated magnetic form factor (11). It was not possible to refine the Mn(*a*) and Mn(*b*) moments independently. The refined components of the magnetic moment were $\mu_x = 1.4(2)$, $\mu_y = 3.7(1)$, and $\mu_z = -0.6(2)\ \mu_B$, and the resultant moment has magnitude 4.0(1) μ_B, consistent with high spin $3d^4$ Mn^{3+}, and similar to the refined values for $RbMnHP_3O_{10}$ and $CsMnHP_3O_{10}$ (5, 7). A good fit to the magnetic peaks is obtained (Fig. 3b) despite the presence of a small amount of secondary phase.

DISCUSSION

The $AMnHP_3O_{10}$ structure is stabilized by the large cations A = K, Rb, and Cs although the three phases all have differently distorted variants of the basic framework. The triclinic $KMnHP_3O_{10}$ structure is the lowest symmetry arrangement. The low resolution of the present powder neutron diffraction data leads to a low precision in the refined atomic coordinates and the derived bond distances (Tables 1 and 2). Taking the usual convention that the calculated standard deviations underestimate true values by a factor of at least three, then the given bond distances can only be considered reliable to within ± 0.1 Å, so that features such as the geometry of the triphosphate group are not clear. The K ion is in 10-fold coordination, but the K–O distances show a bimodal distribution with five short (2.7–2.9 Å) and five long (3.3–3.5 Å) contacts. This can be compared to the Rb (two short (2.8 Å), six intermediate (3.1–3.3 Å) and two long (3.7 Å)) and Cs (eight short (3.1–3.4) and two long (3.7 Å)) environments in the related structures, showing that the coordination becomes less regular as the size decreases.

TABLE 3
The Coordinates and Relative Directions of the Eight Mn Spins in the $a_K \times 2b_K \times 2c$ Magnetic Supercell of $KMnHP_3O_{10}$

Site	x	y	z	Spin	Site	x	y	z	Spin
Mn(*a*)	0	0.75	0.5	+	Mn(*b*)	0.5	0.5	0.25	+
Mn(*a*)	0	0.25	0.5	−	Mn(*b*)	0.5	0	0.25	−
Mn(*a*)	0	0.75	0	−	Mn(*b*)	0.5	0.5	0.75	−
Mn(*a*)	0	0.25	0	+	Mn(*b*)	0.5	0	0.75	+

The structures of $RbMnHP_3O_{10}$ and $CsMnHP_3O_{10}$ contain a single Mn site which is surrounded by a typical Jahn–Teller [2 + 2 + 2] distorted octahedron with two Mn–O bond distances of 1.92, 1.98, and 2.21 Å and 1.89, 1.94, and 2.16 Å, respectively. The triclinically distorted $KMnHP_3O_{10}$ structure contains two Mn sites of which Mn(*a*) again has a [2 + 2 + 2] distorted environment (1.8, 2.0, and 2.3 Å) but Mn(*b*) appears to have an unusual [2 + 4] coordination with two short (1.8 Å) and four long (2.1 Å) bonds. Further refinements using more highly resolved data are needed to confirm the type and magnitude of these distortions.

$KMnHP_3O_{10}$ differs from the Rb and Cs analogues in having a ferromagnetically ordered moment below $T_C =$ 15 K, whereas the other two materials are purely antiferromagnetic. The magnetic structure of $KMnHP_3O_{10}$ is also more complex in having a doubled periodicity in the c direction arising from a different spin arrangement in the $b_{Rb}c$ plane (Fig. 4). In $RbMnHP_3O_{10}$ and $CsMnHP_3O_{10}$ the spins in this plane are aligned ferromagnetically, whereas in $KMnHP_3O_{10}$ they have an antiferromagnetic arrangement. Both the Mn(*a*) and Mn(*b*) sublattices are antiferromagnetic so that the net moment cannot be explained by a simple ferrimagnetism arising from opposing but unequal Mn(*a*) and Mn(*b*) spins or by the possibility that the Mn(*a*) spins are not collinear with those at the Mn(*b*) sites. Weak ferromagnetism due to slight canting of the sublattice moments is often found in low symmetry transition metal oxosalts, e.g., β-$CrAsO_4$ (12) and $Li_2Fe_2(MoO_4)_3$ (13), but this is symmetry-forbidden when the moments are related by an inversion center of symmetry as is the case for all Mn(*a*)–Mn(*a*) and Mn(*b*)–Mn(*b*) interactions in the refined $P\bar{1}$ structure of $KMnHP_3O_{10}$. However, if the true symmetry is $P1$ then this restriction no longer holds, so that a plausible explanation for the net moment in $KMnHP_3O_{10}$ is that weak ferromagnetism arises from spin canting within

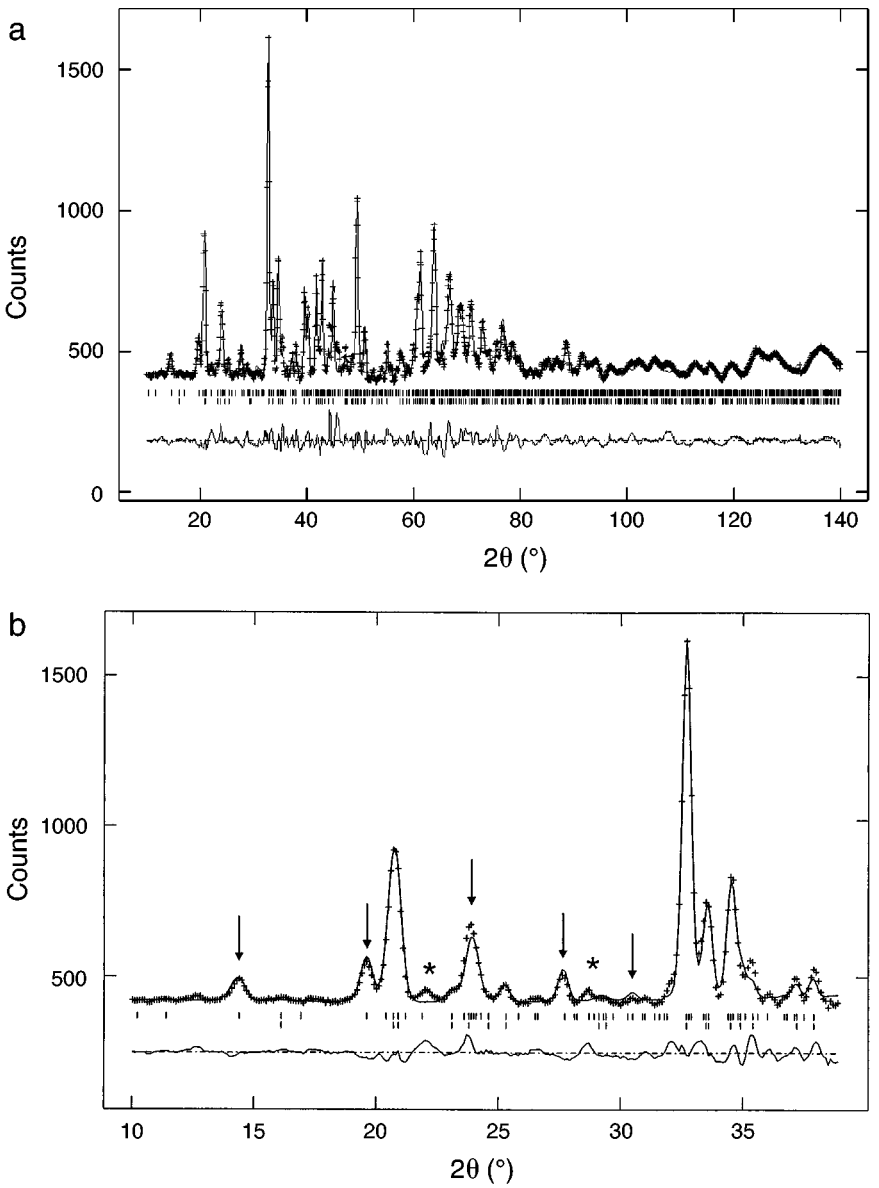

FIG. 3. Observed (+), calculated (full line), and difference powder neutron diffraction profiles of $KMnHP_3O_{10}$ at 2 K (upper markers for magnetic reflections, lower for nuclear): (a) shows the full profile and (b) contains the low angle region with magnetic peaks marked with arrows and those due to a secondary phase marked with (*).

an acentric structure. Canting by $\sim 4^\circ$ from the antiparallel arrangement accounts for the observed ferromagnetic moment.

In conclusion, the three $AMnHP_3O_{10}$ phases (A = K, Rb, Cs) all have different structural symmetries. The monoclinic Rb and Cs materials have the same Jahn–Teller distortion around the Mn^{3+} site and identical antiferromagnetic structures at low temperatures. However, the smaller K cation switches the framework to a lower triclinic symmetry in which two, differently distorted MnO_6 octahedra are present. (The same change from monoclinic symmetry with one Mn site to triclinic with two sites is observed in the $MnAsO_4.H_2O \rightarrow$ LiMnAsO4(OH) transformation (2).) The switch of orbital ordering also leads to a switch in magnetic order, from antiferromagnetic with a simple collinear arrangement for A = Rb and Cs to weakly ferromagnetic with a more complex magnetic structure for A = K. A further high-resolution neutron diffraction study will be needed to determine the precise structure and fully rationalize the magnetic properties of $KMnHP_3O_{10}$.

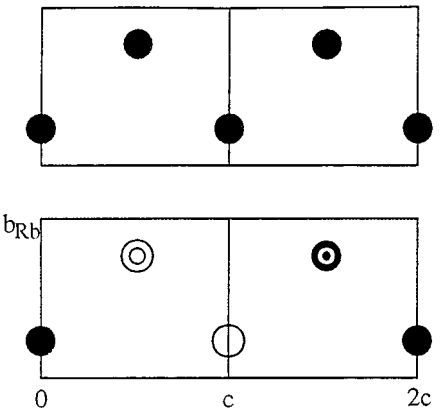

FIG. 4. Comparison of the magnetic structures of $RbMnHP_3O_{10}$ (top) and $KMnHP_3O_{10}$ (bottom) viewed on the [100] plane (using the $RbMnHP_3O_{10}$ cell axes). Filled/open circles represent $+/-$ relative spin directions for Mn atoms in the $x = 1/4$ plane. Structurally inequivalent Mn(*a*)/Mn(*b*) sites in $KMnHP_3O_{10}$ are represented by single/double circles.

ACKNOWLEDGMENTS

We thank Dr. P. Radaelli for assistance in the collection of neutron data and EPSRC for the provision of neutron facilities and Grant GR/K75040. Magnetic susceptibility measurements were made at the Cambridge IRC in Superconductivity.

REFERENCES

1. C. J. Simmons, M. A. Hitchman, H. Stratemeier, and A. J. Schultz, *J. Am. Chem. Soc.* **115,** 11,304 (1993).
2. M. A. G. Aranda, J. P. Attfield, and S. Bruque, *J. Chem. Soc., Chem. Commun.* 604 (1991).
3. M. A. G. Aranda, J. P. Attfield, S. Bruque, and R. B. Von Dreele, *J. Chem. Soc., Chem. Commun.* 155 (1994).
4. L. S. Guzeeva and I. Tananaev, *Inorg. Mater.* **24,** 538 (1988)
5. A. J. Wright and J. P. Attfield, *Inorg. Chem.* **37,** 3858 (1998).
6. E. V. Murashova and N. N. Chudinova, *Kristallografiya* **40,** 476 (1995).
7. A. J. Wright and J. P. Attfield, *J. Solid State Chem.* **141,** 160 (1998).
8. M. T. Averbuch-Pouchot, A. Durif, and J. C. Guitel, *Acta Crystallogr., Sect. B* **33,** 1436 (1977).
9. N. Anisimova, M. Bork, R. Hoppe, and M. Meisel, *Z. Anorg. Allg. Chemie.* **621,** 1069 (1995).
10. A. C. Larson and R. B. Von Dreele, Los Alamos National Laboratory Report No. LA-UR-86-748, 1994.
11. P. J. Brown, "International Tables for Crystallography" (T. Hahn, Ed.), Vol. C, p. 391. Kluwer Academic, Dordrecht, 1992.
12. J. P. Attfield, A. K. Cheetham, D. C. Johnson, and C. C. Torardi, *Inorg. Chem.* **26,** 3379 (1987).
13. W. M. Reiff, J. H. Zhang, H. Tam, J. P. Attfield, and C. C. Torardi. *J. Solid State Chem.* **130,** 147 (1997).